ADVANCED BIOSYSTEMS

Supporting Information

for *Adv. Biosys.*, DOI: 10.1002/adbi.201800101

Stereolithographic 4D Bioprinting of Multiresponsive Architectures for Neural Engineering

*Shida Miao, Haitao Cui, Margaret Nowicki, Lang Xia, Xuan Zhou, Se-Jun Lee, Wei Zhu, Kausik Sarkar, Zhiyong Zhang, and Lijie Grace Zhang**

Supporting Information

Stereolithographic 4D bioprinting of multi-responsive architectures for neural engineering

*Shida Miao,[†] Haitao Cui[†] Margaret Nowicki, Lang Xia, Xuan Zhou, Se-jun Lee, Wei Zhu, Kausik Sarkar, Zhiyong Zhang, and Lijie Grace Zhang**

[†]S. Miao and H. Cui contributed equally to this work

S1. The mechanism of strand bending

Volume shrinkage is a common phenomenon in UV-curing processes. High concentration of double bonds usually results in higher volume shrinkage. Polymerization of acrylate soybean oil epoxide will have obvious volume shrinkage due to the replacement of long-distance connections via weak Van der Waals force by strong short covalent bonds between carbon atoms of different monomer units. Volume shrinkage is usually considered a drawback since it causes problems such as a large build-up of internal stress, resulting in dimensional changes and decreased mechanical properties. Here, our 4D SL printing leads to a nonuniform volume shrinkage, generating internal stress, which can be used to drive the 4D dynamic process. The printing process is shown schematically in **Figure S1**, where the laser light is projected into the SOEA resin. Since SOEA resin has a light yellow color, it is common knowledge that light intensity will decrease with increasing optical depth in SOEA. As indicated in the Beer-Lambert law:

$$A = log_{10}\frac{I_0}{I} = \varepsilon lc$$

Where *A* is light absorbance,

Given a specific substance, the absorbance of the light will increase as the optical depth *l* increases. Thus, the surface facing laser head (closer to laser head) will have highest cross-linking density while the surface opposite to laser head will have lowest cross-linking density, as shown in **Figure S1**.

In this process, light intensity is continuous, but the internal stress induced 4D shape change can be better explained using the layer concept. When the laser light passes over the SOEA resin, the layer directly exposed to laser light will be cured immediately, whereas the layer adjacent to this layer is

not sufficiently polymerized and still in liquid state. Due to the presence of laser light intensity gradient, volume shrinkage happens in a sequential manner. That is, the earlier cured layer shrinks first, whereas subsequently cured layer shrinks under the confinement of the early cured layer. As a result, a nonuniform stress filed is developed across the thickness of the printed strand. The early cured layer has a compressive stress while the newly cured layer has tensile strength. Thus, the printed strand has a tendency to bend toward the newly cured layer, which aligns with our observation in experiments and is indicated in Figure S1. The internal stress generation process in our 4D SL printing is very similar with the internal stress generation in frontal polymerization (Zhao et al., Sci. Adv. 2017; 3: e1602326). In the reported frontal polymerization, the resin is transparent and colorless; thus photoabsorbers are added to enhance an intensity gradient in the resin. Another difference is that the sample is formed on a substrate in the frontal polymerization. The sample still remains flat in shape after it has internal stress gradient due to the restriction from the substrate. Once the sample is moved from the substrate, the internal stress is released, driving the dynamic shape change. In our 4D SL printing, the laser is directly exerted on the resin and there is no substrate to constrict the shape. But there is no shape change during printing process; the printed strand still keeps flat even after taken out of the resin. We assume that the high sticky feature of SOEA prevent the release of internal stress. Thus, the release of internal stress is initiated by immersing the sample in ethanol in our study. When the printed sample is immersed in ethanol, the unsolidified resin on the surface of the sample will be dissolved; ethanol also provides a liquid environment which is easy for shape change. Then the internal stress will be released and 4D dynamic shape change will be observed in several seconds.

Figure S1. The internal stress in the printed strand and shape change direction

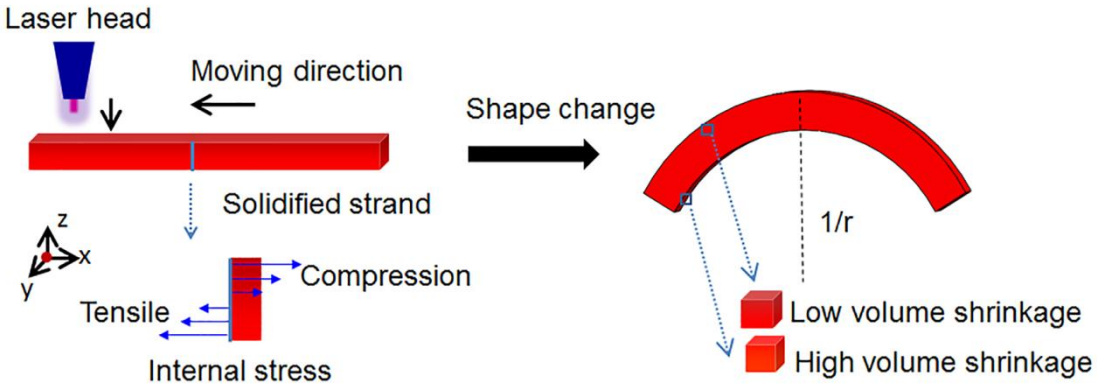

S2. The thickness of the printed strand vs printing speed

The printing speed has a significant effect on the thickness of the strand. As the printing speed increases, the thickness of the strand decreases markedly (**Figure S2**).

Figure S2. The effect of printing speed on the thickness of the strand

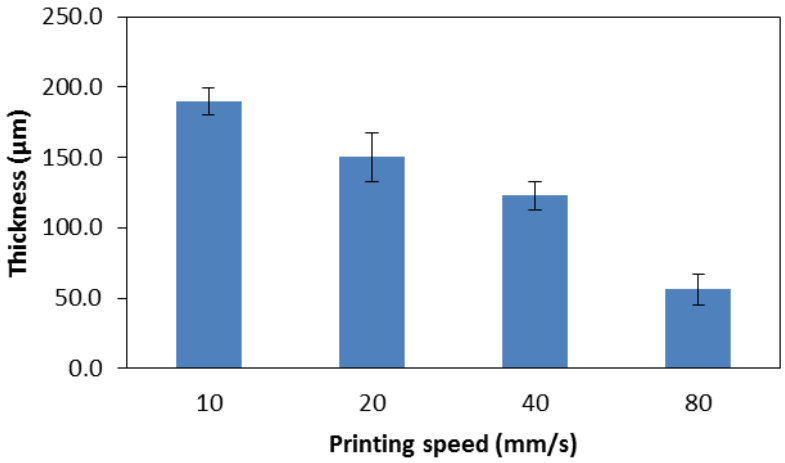

S3. Modeling of the 4D dynamic process

(S3-1) Polymerization of the strand

The process of polymerization alters the physical properties of the material and induces the volume shrinkage as well. The portion that receives more light energy will have more solidification and thus more mechanical strength (e.g., higher Young's modulus); whereas the portion that receives less light energy will get less polymerization and less mechanical strength, resulting in the strand analog to a functionally graded beam. Partial polymerization also leads to formations of the porous structure where pores are filled with uncued resin. These uncured resins balance the inner stress due

to the shrinkage of the polymerization. When the strand is immersed in ethanol, the ethanol invades the porous structure, gradually dissolving the resins inside the pores. The stress-strain balance is thus broken, and the strand starts to deform immediately. At the same time, the ethanol diffuses into the pores and soaks the bent strand, of which the effect counteracts the bending. This process may be characterized by flows in porous media with mass transfer and affected by a number of factors, such as pore size, pore volume fraction, diffusion rate, and dissolution rate/solubility of the resins. It is thus rather complicated. We are going to build a simple mechanical model with some linear assumptions to help illustrate this phenomenon.

(S3-2) Relation between the printing speed and the strand thickness

The thickness of the printed strand depends on the printing speed, as shown in **Figure S3**. It is related to the energy offered by the laser. The higher the printing speed, the less the exposure time of the material and thereby the less polymerization, leading to the thinner the material. The polymerization thickness is affected by multiple factors. To simplify the modeling, we may just assume the validity of following relation:

$$h = Q \ln \frac{\alpha}{v} \text{ [m]} \qquad (1)$$

Here Q with a unit of length is a physical constant, α is another constant with a velocity unit, and v is the printing speed.

Using the above equation and fitting to the following data,

Figure S3. Printing speed vs. thickness. Scattered squares are experimental data, the gray curve is the prediction from Eq.(1).

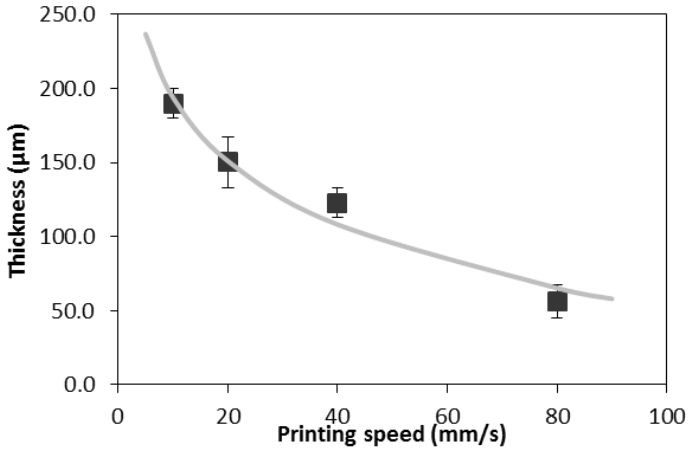

we have $Q = 61.86\times10^{-6}$ m, and $\alpha = 0.23$ m/s.

(S3-3) Relation between curvature and printing speed

(S3-3-1) Bending in ethanol

Here the relationship between the curvature and printing speed can be modeled using the following equation (See detailed derivations in S3-4) (**Figure S4**)

$$\frac{1}{r} = -46.88\frac{\chi_0}{1.47+\ln v}\ [\mathrm{m}^{-1}] \qquad (2)$$

where χ_0 is the shrinkage depending on the material and the immersed medium. Here $\chi_0 = 0.019\ \mathrm{s}^{-1}$ [1] for ethanol. The above simple equation correlates the curvature of the strand to other controllable parameters, which could help print objects of desirable shapes. More interestingly, the Young's modulus does not contribute to the final curvature directly. It is their difference and ratio *D* that make a difference. This is mainly due to the linear assumption on the Young's modulus.

Figure S4. Printing speed v.s. curvature. Gray curves are predictions from Eq.(2).

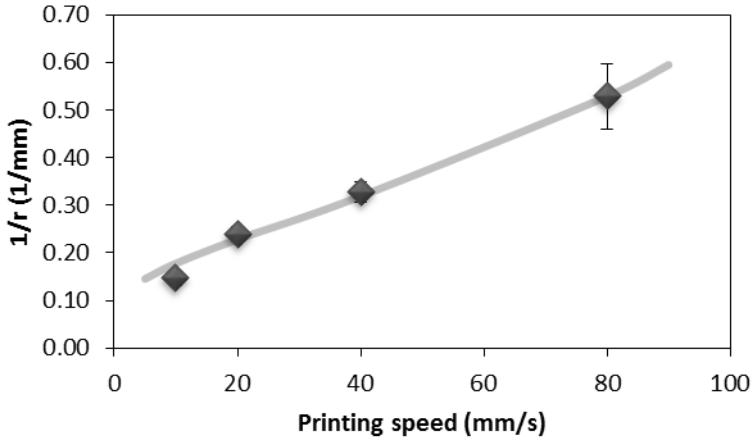

(S3-3-2) Flatting in Ethanol

The flatting of the strand can be modeled by the following relation (**Figure S5**)

$$\frac{1}{r} = c_0 \ [\mathrm{m}^{-1}] \tag{3}$$

Here the constant $c_0 = 60.51\ \mathrm{m}^{-1}$ is obtained from fitting experimental data.

Figure S5. Printing speed vs. curvature. Gray curves are predictions from Eq.(3).

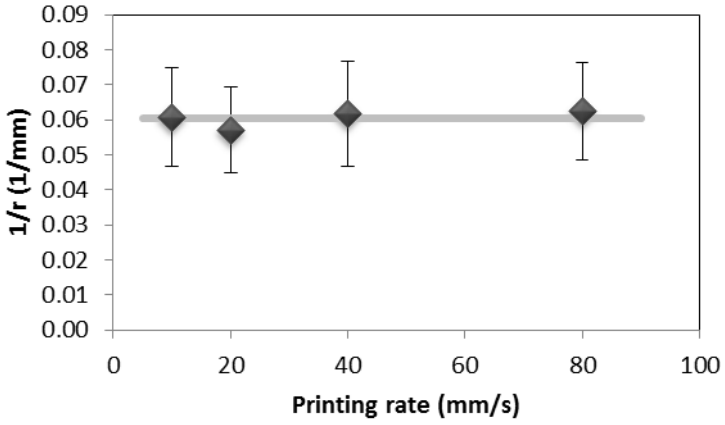

(S3-3-3) Bending in Water

When the strand is immersed in the water, the ethanol inside the strand diffuses out. However, water is not able to penetrate into the pores due to the extremely high surface tension and hydrophobicity of the soybean based material. The loss of ethanol results in the bending of the strand again. Therefore, we have the same equation for evaluating the curvature, that is:

$$\frac{1}{r} = -46.88\frac{\chi_0}{1.47 + \ln v} \ [\mathrm{m}^{-1}] \tag{4}$$

Here $\chi_0 = 0.012\ \mathrm{s}^{-1}$ for water (**Figure S6**).

Figure S6. Printing speed vs. curvature. Gray curves are predictions from Eq.(4).

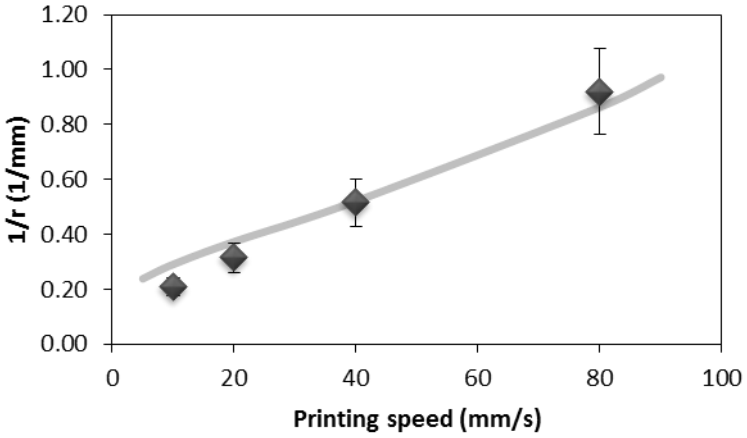

(S3-4) Derivations

Figure S7. Schematic representation of the strand as a graded Euler-Bernoulli beam.

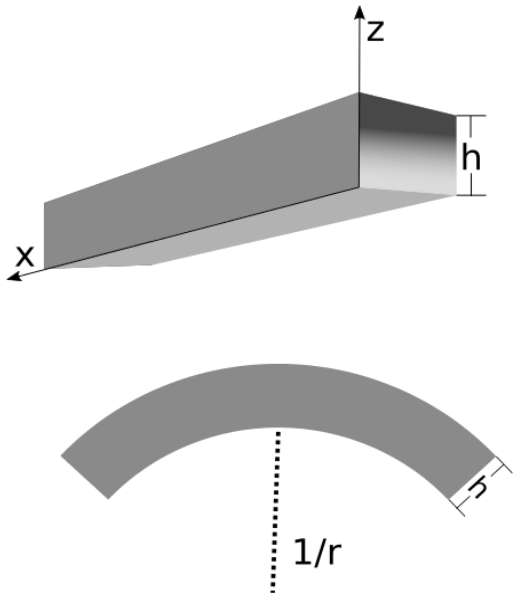

(S3-4-1) Stress-strain relation

We do not consider the dynamics of the strand. We only consider the final state of the deformed strand. Therefore, the problem is simplified to static analysis. When applying the Euler-Bernoulli beam to the current study, the strain due to bending may be written as

$$\varepsilon(z) = \varepsilon_s(z) + kz \qquad (5)$$

Here $\varepsilon_s(z)$ is the strain due to shrinkage of the polymer beam, z is along the direction of thickness, and k is the curvature of the bending beam.

Note that in polymerization literature, the shrinkage refers to volume shrink caused by photocuring. In the present study, however, the shrinkage is a post-curing effect due to the immersion of liquids,

rather than due to the light exposure. The material's properties are very much dependent on the laser's intensity, if we assume the intensity of the laser light attenuates exponentially in the *z* direction (obeys the aforementioned Beer-Lambert law), we may also write the shrinkage strain in the following form

$$\varepsilon_s(z) = \chi_0 \exp(-Az) \tag{6}$$

Here χ_0 is the shrinkage at the bottom of the beam, and *A* is a coefficient determined the properties of the material. Although *A* is interpreted as light absorption or attenuation as shown in **S1-3**, its determination still requires knowledge of the medium. Here, we are able to calculate the value of *A* in terms of the present model. The total strain may be written as

$$\varepsilon(z) = \chi_0 \exp(-Az) + kz \tag{7}$$

As for the stress, noticing the fact that Young's modulus varies with respect to *z*, we may use linear relation of the following form

$$E(z) = E_b + \frac{E_t - E_b}{h} z = E_b \left(1 + \frac{D}{h} z\right) \tag{8}$$

where $E_b = 37.3\,\text{MPa}$ and $E_t = 75.1\,\text{MPa}$ are the Young's moduli on the bottom and top surfaces, respectively. *h* is the thickness of the beam and $D = (E_t - E_b)/E_b$.

Finally, the stress can be expressed by

$$\sigma(z) = E(z) \cdot \varepsilon(z) \tag{9}$$

Substitute Eq.(7) and Eq.(8) into Eq.(9), we have

$$\sigma(z) = E_b \left(1 + \frac{D}{h} z\right)\left(\chi_0 \exp(-Az) + kz\right) \tag{10}$$

(S3-4-2) Balance of force and bending moment

At the equilibrium state, we have

$$\begin{cases} \int_0^h \sigma(z)\, dz = 0 \\ \int_0^h \sigma(z)\, z dz = 0 \end{cases} \tag{11}$$

Substitute Eq.(10) into Eq.(11) and integrate along the *z* direction

$$k = -6\chi_0 \frac{Ah + D - \left(ADh + Ah + D\right)e^{-Ah}}{A^2\left(2D+3\right)h^3}$$
$$k = -12\chi_0 \frac{Ah + 2D - \left(A^2Dh^2 + A^2h^2 + 2ADh + Ah + 2D\right)e^{-Ah}}{A^3\left(3D+4\right)h^4} \quad (12)$$

Solving the above equations will render the expression of *A*. When the beam is thin, we can use the approximation $e^{-Ah} \approx 1 - Ah$ and then obtain

$$A = -\frac{2D\left(2D+3\right)}{\left(3D+4\right)h} \quad (13)$$

Therefore, the curvature is in the form of

$$k = -\frac{6\left(4D^2+9D+4\right)}{\left(6D^2+17D+12\right)}\frac{\chi_0}{h} \quad (14)$$

with the help of Eq.(1), we have

$$k = -\frac{6\left(4D^2+9D+4\right)}{6D^2+17D+12}\frac{\chi_0}{Q\ln\frac{\alpha}{v}} \quad (15)$$

Note that $k = -1/r$, where *r* is the radius of the curvature.

(S3-4-3) Relaxation Process

When the strand further stays in ethanol, the liquid diffuses into the porous structure and reduces the strain inside the strand. This process may be described by the diffusion equation and Darcy's law in porous media. Here we simplify the analysis by the introduction of relaxation of the strain, and thus a new equilibrium can be achieved. At this state, we may assume the strain linearly depends on the z, therefore

$$\varepsilon_s(z) = c_0 z + kz \quad (16)$$

Using Eq.(13) again, we have

$$k = -c_0 \quad (17)$$

which gives constant curvature for the final deformation of the strand in ethanol.

The current analysis is restricted to the static balance of force and moment. As for the modeling of the evolution of the curvature, we may need to consider more complicated equations such as mass transfer and flows in porous media, to better characterize the evolution. It is definitely the direction of our future work.

S4. The pattern design for the 4D printing

In the first three columns in **Figure S8**, the printed flowers are expected to bend-up directly. In the fourth column, the printed flower is expected to bend with a 45° angle. The petals of the flower in the first three columns are bending-up directly as expected because of the incorporation of different patterns on the second layer. The flower in the 4th column exhibits a structure as expected.

Figure S8. The structure design for 4D printing

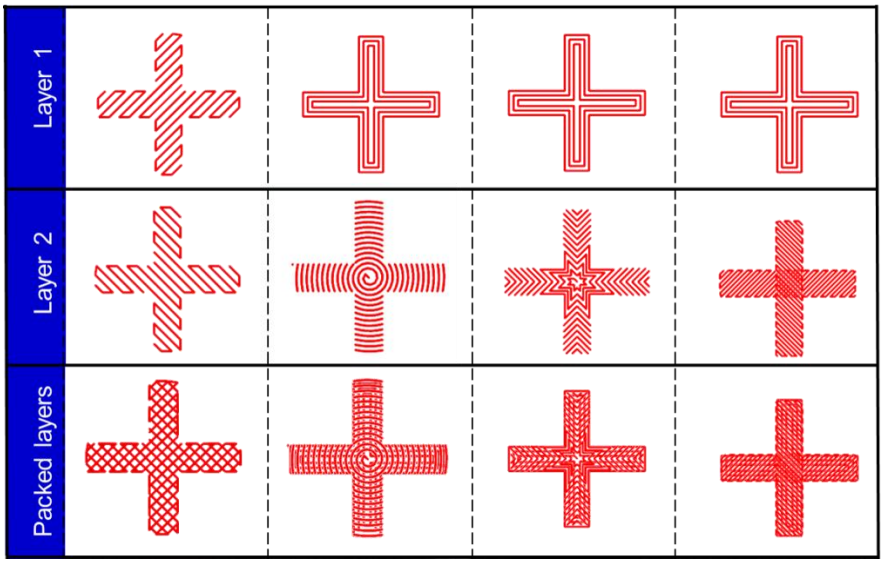

S5. The glass transition temperature (T_g) of the printed sample

The sample is printed at a speed of 40 mm/s with laser intensity of 20k Hz. T_g was measured with a multicell differential scanning calorimeter (MC DSC) from TA Instruments (New Castle, DE) at a programmed ramp rate of 1°C/min. The sample was first heated from 25 °C to 150 °C and held at 150 °C for 1 min. Next, the sample was cooled from 150 °C to -30 °C and held at -30 °C for 1 min. A second cycle was conducted: heating from -30 °C to 150 °C, holding 1 min and decreasing from

150 °C to -30 °C where results from this second cycle were used to determine the T_g. The DSC curve is shown in Figure S9.

Figure S9. The DSC curve of the printed sample.

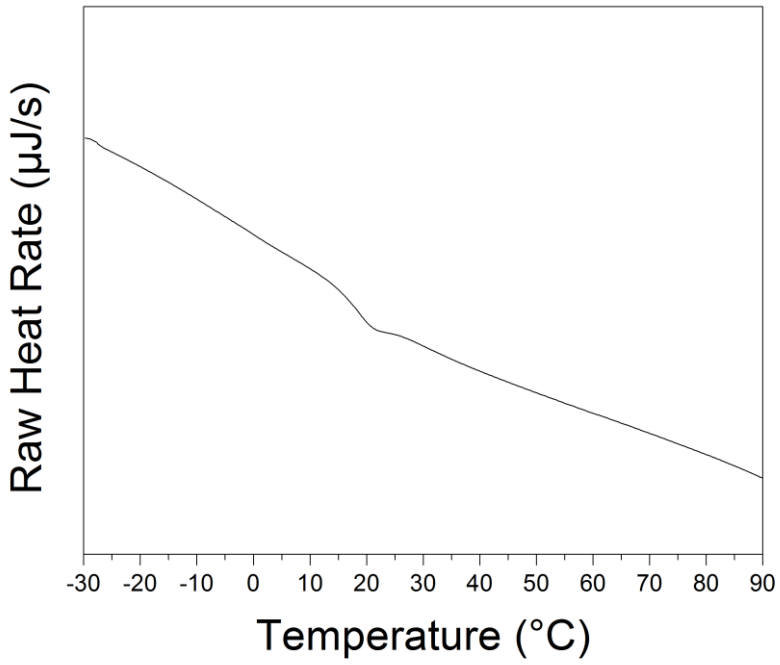

S6. The effect of nanomaterials on the curving of the printed strands

Four nanomaterials are used to print the structures; they are NanoFe_2O_3 (iron (III) oxide, magnetic, 20-40 nm APS powder), Carbon nanofibers (D×L, 100nm × 20-200 μm), nHA (nano hydroxyapatite, 100 nm), and Graphene (1-2 μm diameter). Compared to the Soy control, four types of nanomaterials (0.8%) can increase the curving of the printed structure markedly (printing speed 10 mm/s; laser intensity 20000 Hertz), as shown in **Figure S10-a**. The micro-surficial structures of the printed strand are shown in **Figure S10-b**. Microporous structures are clearly observed. Similar with the graded cross-linking density along the attenuating direction of laser light, the micro-surficial structures are located on the downside, which is farther from the laser head. This uneven structure is assumed to be the factor which increases the curvature of printed strand.

Figure S10. (a)The scaffolds printed with different nanoinks; printing speed 10mm/s; laser intensity 20000 Herz. (b)SEM photos of the surficial structures of the printed strands.

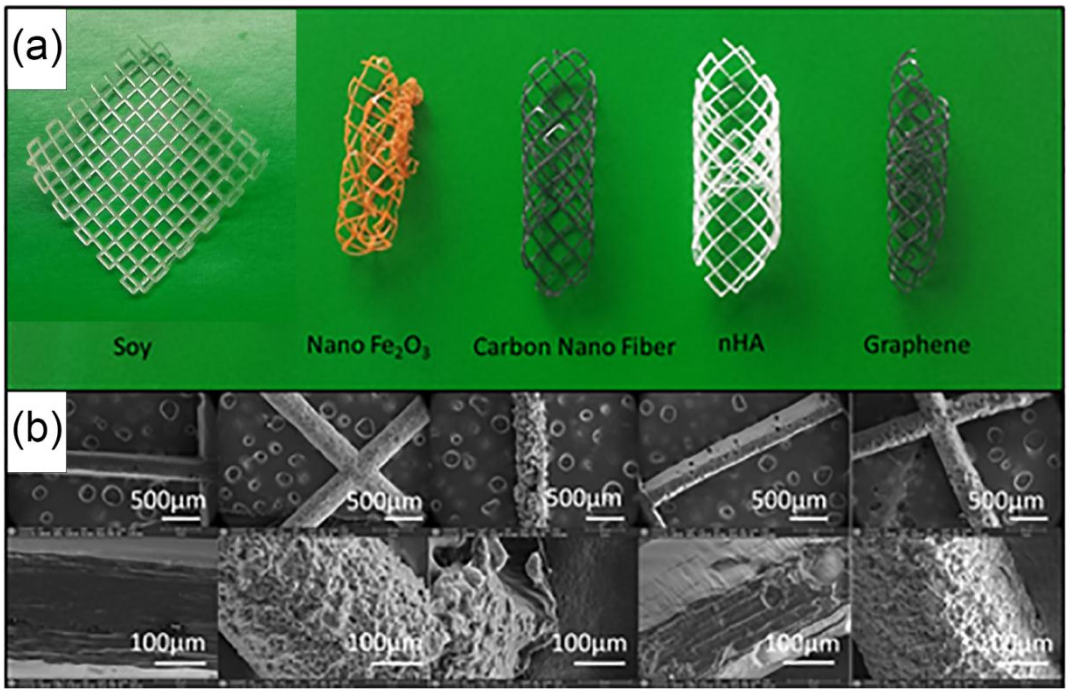

The addition of graphene also affects the thickness of the printed strands as shown in **Figure S11**. While the distance of laser to ink surface has a small effect on the strand thickness, the addition of 0.8% graphene decreases the thickness more than 50%. However, the graphene sample shows higher curvature than the non-graphene sample when they have the same thickness (**Figure S12**). The enhanced curving by graphene may be due to the nano-material induced porous surficial structure as shown in Figure S10.

- *Figure S11. The effect of graphene on the thickness of printed strands.*

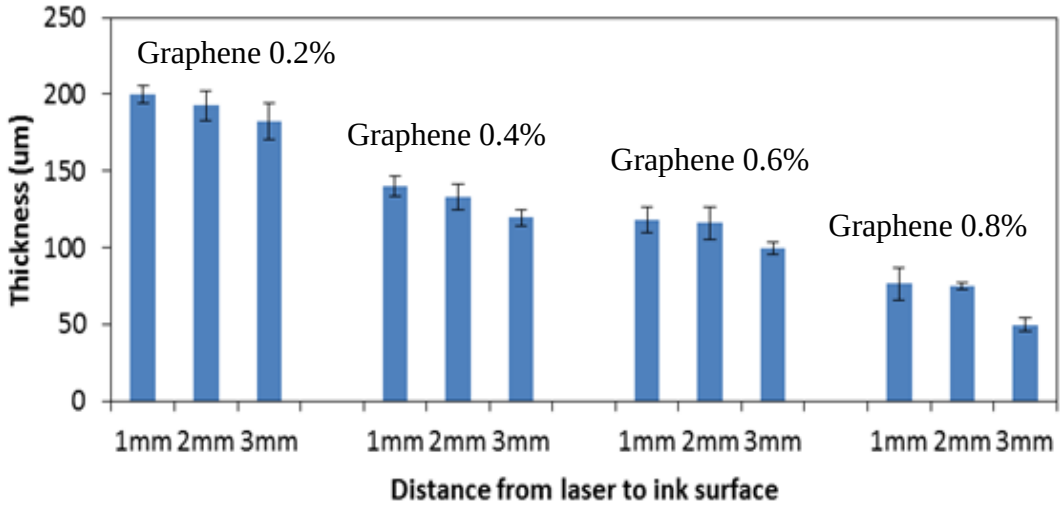

Figure S12. The curvatures of the graphene-containing sample and non-graphene sample when they have same thickness.